Optimal operation and conceptual design of a novel façade-integrated adsorption cooling system

Simon O. Weber[1], Olaf Böckmann[2], Andreas Greiner[3], Sumee Park[4], Micha Schäfer[2], Martin Ostermann[3] and Philip Leistner[1]

[1] Institute for Acoustics and Building Physics, University of Stuttgart (Germany)

[2] Institute for Building Energetics, Thermotechnology and Energy Storage, University of Stuttgart (Germany)

[3] Institute for Building Construction, University of Stuttgart (Germany)

[4] Fraunhofer Institute for Building Physics, Valley (Germany)

Abstract

About 5% of the world's energy consumption is used for indoor air conditioning Construction (UN 2021 Status Report). This study expects it to increase by up to 157% by 2050 under stated policies scenario. This could be accompanied by an increasing risk of power outages. To meet the enormous summer cooling demand of buildings, a component is therefore needed that provides cooling energy off-grid and emission-free. The façade-integrated adsorption cooling concept presented in this paper provides cooling energy in a decentralized and nearly emission-free way. By using this concept, large pipe routes can be dispensed with, the use of environmentally harmful coolants can be avoided, and power generation peaks can be reduced. For this purpose, an optimization-based operation strategy for a novel adsorption cooling system is presented in this paper. In addition, to support an optimal conceptual design, the critical building parameters are identified, their number is reduced and varied with respect to energy efficiency.

By applying a novel operation strategy, the system can be controlled more efficiently and in a more comprehensive adsorber orientation range compared to the previous operation strategy. In this context, the reduction of power consumption on the hottest day of the year shows a strong dependence on the adsorber orientation and the area ratio of the adsorption cooling components. In the optimal parameter configuration and using the new operating strategy, the power consumption can be reduced by 70%.

Keywords: optimal operation, conceptual design, façade integration, adsorption cooling

1. Introduction

According to the UN's recently published 2021 Global Status Report for Buildings and Construction (UN 2021 Status Report), the building sector contributes 37% of global carbon dioxide emissions and 36% of global energy consumption. Building cooling accounts for 5% of energy consumption annually. In addition, global energy demand for building cooling will increase between 29% to 157% by 2050, depending on the stated policies scenario. This could be accompanied by an increase in the risk of power outages. On the one hand, due to the simultaneous supply of the increasing cooling demand and, on the other hand, due to the drought-induced shutdown of power plants.

Within this background, the Collaborative Research Centre 1244 (CRC 1244) at the University of Stuttgart interdisciplinary investigates adaptive building skins and structures to reduce resource consumption in building construction as well as energy consumption in building operation. Based on the results of the first research phase, the world's first adaptive high-rise experimental building (D1244) was inaugurated this year (Blandini et al., 2022). They showed that lightweight adaptive buildings can reduce the greenhouse gas emissions over the entire life cycle (material + operation) by 40%. Unlike conventional massive buildings, lightweight buildings have low inherent thermal capacity and thus are prone to thermal oscillations.

doi:10.18086/eurosun.2022.06.11 Available at http://proceedings.ises.org

The novel façade-integrated adsorption cooling system used in this work relies on the previous work of Boeckmann et al. (2021) and Heidingsfeldt et al. (2022). It addresses several challenges at a time by offering the possibility to provide energy for building cooling in a nearly climate-neutral and decentralized way and by refraining from the use of environmentally harmful coolants. Thus, it contributes to the reduction of emissions in construction and operation as well as to grid resilience.

Prieto et al. (2017) and Almasri et al. (2022) supply a broad overview on current work on façade-integrated cooling and solar sorption cooling systems, respectively. Accordingly, solar energy is either converted into electricity in PV modules or into heat in solar collectors. From that cooling energy is mainly generated by using compression or sorption chillers, respectively. In the group of solar thermal cooling systems, which are studied widely, the most installations are either absorption or adsorption systems (Settino et al., 2016). The systems presented in the quoted technology overview have separated solar thermal collectors and sorption units, which are usually placed on the building's roof or in the basement. In contrast to these systems, the adsorption system in this work combines the adsorber and the solar collector into one component, which allows it to be façade integrate able. This is favourable due to the high potential of solar energy harvesting in this area. Furthermore, the integration into the façade reduces the competition for space on the roof surface between HVAC systems, photovoltaics, terrace use or greenspace applications.

The integration into the facade also leads to certain challenges. For example, the adsorber orientation must be adapted to the location. The mutual dependence of the adsorber orientation, the switching times of the operating phases and the cooling demand in the room must be coordinated. This requires a control concept that can consider the influencing factors presented. The current control concept, in the following called rule-based strategy, switches the phases based on predefined heuristics. External signals such as the solar energy input and internal states such as the pressures of the individual components are considered. This results in the main tasks of this work. In addition to the development of an optimization-based operating strategy of the facade-integrated adsorption cooling system, an efficiency analysis of selected system parameters is carried out. The discussion of the simulation results focusses on the following hypotheses:

- The optimisation-based operation strategy enables lower power consumption than the rule-based strategy
- The performance of the system strongly depends on the building orientation as well as the area ratio of the components

The paper is organized as follows: In Section 2, the models of the adsorption cooling, the additional compression cooling, the air conditioning system, and the building are described. Furthermore, the control strategies of the total system and the adsorption cooling are explained and the parameters for the parametric study are introduced. The simulation results are presented and discussed in detail in Section 3. Finally, the study is concluded in Section 4.

2. Methods

The system consists of the building and the HVAC equipment. This includes the heat pump (HP), ventilation (AHU), compression cooling (COCH) system and the novel facade-integrated adsorption cooling (ADCH) system. All models and controls were created in Dymola with the modelling language Modelica.

2.1. Building

For the building model, the zonal model from the IBPSA library was used. This library forms the core of the validated Modelica building models Aixlib, Buildings, BuildingSystems and IDEAS. The building model was created for one squared building storey of the D1244 high-rise, with an internal ground area of 5.11m x 5.11m and 2.85m height. The variable volume of the evaporator is then subtracted from the room volume V_Z. Weather data were generated for the location of D1244 on the university campus (N 48.749°, E 9.112°) using Meteonorm software. For all results, July 8 was selected as the hottest day of the test reference year.

The building zone is surrounded by four types of facades, whose dimensions are the subject of parameter variation, the floor and roof. The facade types include a lightweight wall, a window wall, the adsorber and condenser components. The lightweight wall is constructed in five layers, their thicknesses and material properties are shown in Table 1. The window-to-frame ratio f_{WF}, the secondary heat gain coefficient q_i and other properties of the window wall are shown in Table 2. The window data were generated for a triple low-e argon glazing and vinyl

frame within the WINDOW 7.8 software. The properties of the adsorber and condenser facade are presented in the subsection 1.c. The floor and ceiling were modelled as a 13cm thick steel-concrete layer ($c_p = 1000\frac{J}{kgK}, \lambda = 2.5\frac{W}{mK}, \rho = 2500\frac{kg}{m^3}$). This corresponds approximately to the dimensions of adaptive ceiling systems, which are investigated within other subprojects of the CRC 1244. The internal and external combined convective-radiative heat transfer coefficients were taken from the EN ISO 6946 standard ($h_{ind} = 7.7\frac{W}{m^2K}, h_{ext} = 25\frac{W}{m^2K}$). The outermost short wave radiation absorption coefficient was set to 0.3.

Table 1: Properties of the lightweight wall

Layer	Material	$s\ [cm]$	$c_p[\frac{J}{kgK}]$	$\lambda[\frac{W}{mK}]$	$\rho[\frac{kg}{m^3}]$
1 / outermost	Plaster lime mortar	2	1000	0.869	1800
2	Medium-density fibreboard	2	1700	0.130	650
3	Mineral wool	10	840	0.032	30
4	Medium-density fibreboard	2	1700	0.130	650
5 / innermost	Plaster gypsum	1.5	1000	0.333	1200

Table 2: Properties of the window wall

$g[-]$	$q_i[-]$	$U[\frac{W}{m^2K}]$	$f_{WF}[-]$
0.279	0.09	0.942	0.1

The building model is influenced by heat flows due to the interaction with the ambient temperature, the solar gains, internal gains, and those heat flows of the HVAC systems. The internal gains are active only in the range of working hours from 7-18h, where 2 people emit the total heat output $\dot{Q}_{IG} = 440W$. This results from the radiative and convective heat flows of each person and the convective heat flow of two PC (DIN V 18599-10 Table A.2).

2.2. Heat pump, ventilation, compression chiller

A simple COP model is used for the heat pump and the compression chiller, cf. equations 1 and 2. The ventilation exchanges the room volume at the given air exchange rate acr with ambient air without heat recovery, cf. equation 3. The EPM Pabst 6312 TDH fan, cf. equation 4, is assumed for the energy consumption of the ventilation. The total energy consumption is then calculated as the integral of all power components over the specified day, cf. equation 5.

$$\dot{Q}_{HP} = COP_{HP}\, P_{HP} \qquad COP_{HP} = 4 \qquad \text{(eq. 1)}$$

$$\dot{Q}_{COCH} = -COP_{COCH}\, P_{COCH} \qquad COP_{COCH} = 3 \qquad \text{(eq. 2)}$$

$$\dot{Q}_{AHU} = \frac{c_{p,air}\,\rho_{air}\,V_Z}{3600}(T_a - T_Z)acr \qquad \text{(eq. 3)}$$

$$acr = 13.55\frac{m^3}{Wh}\frac{1}{V_Z}P_{AHU} \qquad \text{(eq. 4)}$$

$$E_{tot} = \int_0^{24} P_{HP} + P_{COCH} + P_{AHU}\,dt \qquad \text{(eq. 5)}$$

2.3. Façade-integrated adsorption chiller

In contrast to the technical systems mentioned in subchapter 2.b, the novel facade-integrated adsorption system provides cooling without emissions during operation. The cooling system consists of the components adsorber, condenser and evaporator which are vacuum-tight and separably connected by valves. Figure 1 shows the schematic structures of each component. The adsorber contains zeolite as the adsorbent and water as the adsorptive. Zeolite is used because of its well-documented properties. Material optimization is the subject of future

work. To introduce the heat and maintain the vacuum medium, the adsorbate is encased and permeated with aluminium fins. It is decoupled from the interior of the room by a 4cm layer of vacuum insulation panel ($c_p = 1000\frac{J}{kgK}, \lambda = 0.003\frac{W}{mK}, \rho = 150\frac{kg}{m^3}$). An air gap and glazing separate the adsorber from the environment. Switchable dampers are placed at the outlets and inlets of the air gap. The condenser is also encased and permeated with fins. It condenses water vapor and releases the heat to the environment. It is also insulated by a 4cm thick layer of vacuum insulation panel to the room. The evaporator is installed under the ceiling of the room. It is also

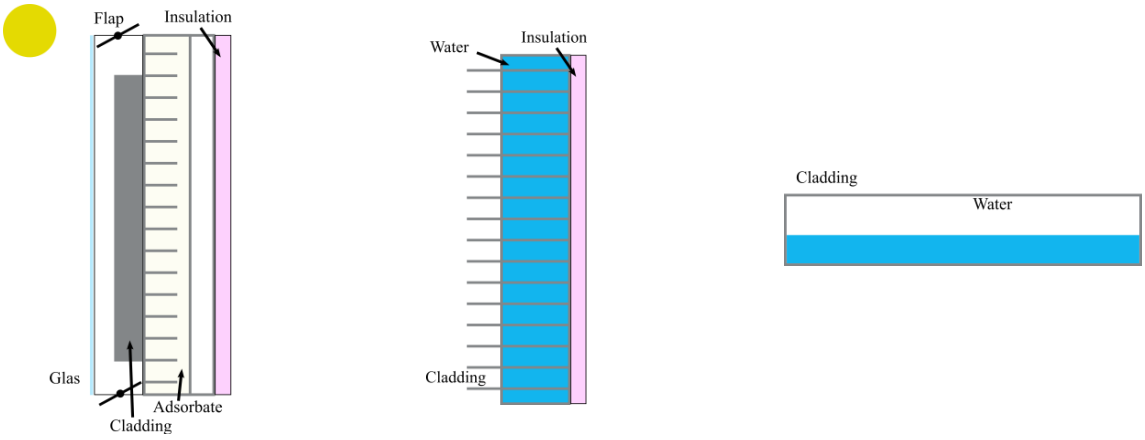

Figure 1: Schematic construction of adsorber (left, side view), condenser (center, top view) and evaporator (right)

encased and extracts the heat necessary for evaporation from the room.

The components are connected to each other by valves depending on the operating phase, cmp. Figure 2. In phase 1, the intermediate heating, all valves are closed and the adsorber is heated up by the absorbed solar radiation. In the subsequent desorption phase, phase 2, the valve from the adsorber to the condenser is opened. Water vapour desorbs out of the zeolite and is liquefied in the condenser. Then follows phase 3, the intercooling phase. During this phase, all valves are closed and the adsorber is cooled down to a lower temperature level. This cooling process is accelerated by opening the dampers. These dampers enable free convective cooling of the air gap in the adsorber. In the actual cooling phase, phase 4, opening the valve between the evaporator and the adsorber starts the adsorption process of water vapour from the evaporator to the zeolite. The dampers are opened to dissipate the heat generated in the process. The evaporation of the water cools it down, whereby heat is extracted from the room via the finned evaporator shell. The implemented model equations for the adsorption system are presented in the paper by Heidingsfeld et al. (2022).

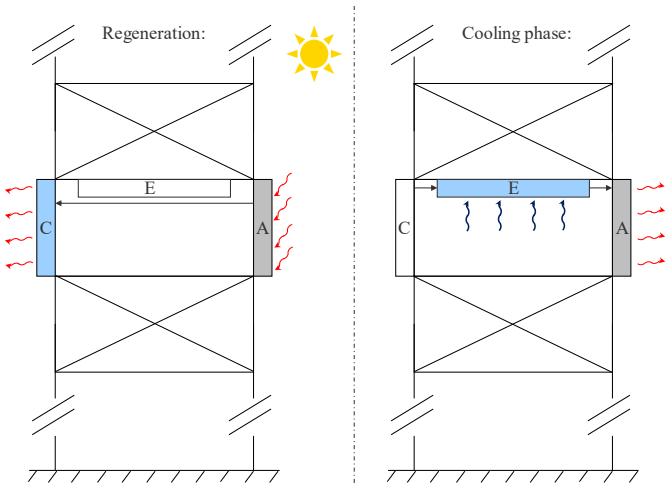

Figure 2: Operation principle of the façade-integrated adsorption cooling system

2.4. Control concept

A control concept was created for the building model, which specifies the control variables of the system and efficiently operates the system. The following manipulated variable and state constraints must be fulfilled. Within working hours, the room temperature must be between $21°C$ and $24°C$ (DIN 18599-10 Table A.2). Outside working hours, the limits are extended by $5K$. In addition, an air exchange rate acr between 2 h^{-1} and 3 h^{-1} must be achieved during working hours. This range was also expanded outside working hours to 0 h^{-1} and 6 h^{-1}. The control concept is shown in Figure 3. In the first link of the control chain, the set point of the total cooling capacity $\dot{Q}^*_{tot}$ is determined from a set point/ actual value comparison of the room temperature. If the room needs to be warmed up, the heating output is transferred to the heat pump. However, this is not necessary for the selected day and is therefore not depicted. In the split unit, the individual systems are added one after the other. First, an attempt is made to achieve the total cooling capacity through the ventilation $\dot{Q}^*_{AHU}$. If this cooling capacity is not sufficient, the adsorption cooling system is given the remaining cooling capacity $\dot{Q}^*_{ADCH}$. Finally, the remaining differential power is set to the compression cooling system $\dot{Q}^*_{COCH}$.

A blind is added to each window. To represent a realistic solar energy input with minimal computational effort, the mitigation factor F_c value was set constant ($F_c = 0.1$) for all blinds. The control variables of the ventilation and compression cooling are the air change rate acr and electric power P_{COCH}, respectively. They are set within their own PID control loops such that the specified setpoint is maintained. The manipulated variables of the adsorption cooling system are the valve positions between the evaporator and adsorber and between the adsorber and condenser, the damper positions dmp in the adsorber air channel and the signal of the pump pmp between the condenser and evaporator. In order not to open the two valves simultaneously, their valve signal is combined. Negative values of the combined signal enable desorption, only the valve to the condenser is opened. In contrast, only the valve from the evaporator to the adsorber is open for positive values vlv. At zero, both valves are closed. The combined valve signal vlv is at zero in phases 1 and 3, at a constant -1 in phase 2 and at 1 in phase 4 if the applied setpoint cooling capacity $\dot{Q}^*_{ADCH}$ is greater than the actual cooling capacity $\dot{Q}_{ADCH}$ from the evaporator. The dampers in the adsorber gap are opened as described above to support adsorber cooling in phases 3 and 4 and are closed in phases 1 and 2. Irrespective of the operating phase, the pump pumps water into the evaporator in the morning hours until a predefined water mass is reached.

Decisive for the control of the valve and the air dampers is the selection of the phases in the SEL_{Phase} block, cmp. Figure 3. Two approaches are compared in this work. The so-called rbd-approach (rule-based) switches the phase starting from phase 1 using fixed switching heuristics. The switching conditions are first published by Heidingsfeldt et al. (2022). With rbd-strategy, the phase is switched from 1 to 2 as soon as the adsorber pressure exceeds the condenser pressure ($p_{ads} > p_{con}$). Intercooling starts as soon as the irradiation drops ($\dot{G}_s < 0$), the irradiation on its surface is below a threshold ($G_s < 200$) and the adsorber loses more heat than it receives ($\Delta\dot{Q}_{ads} < 0$). The cooling phase 4 starts if the evaporator pressure exceeds the adsorber pressure ($p_{eva} > p_{ads}$) and steps to intermediate heating with the sunrise at the next morning ($\dot{G}_s > 0$ & $G_s > 0$).

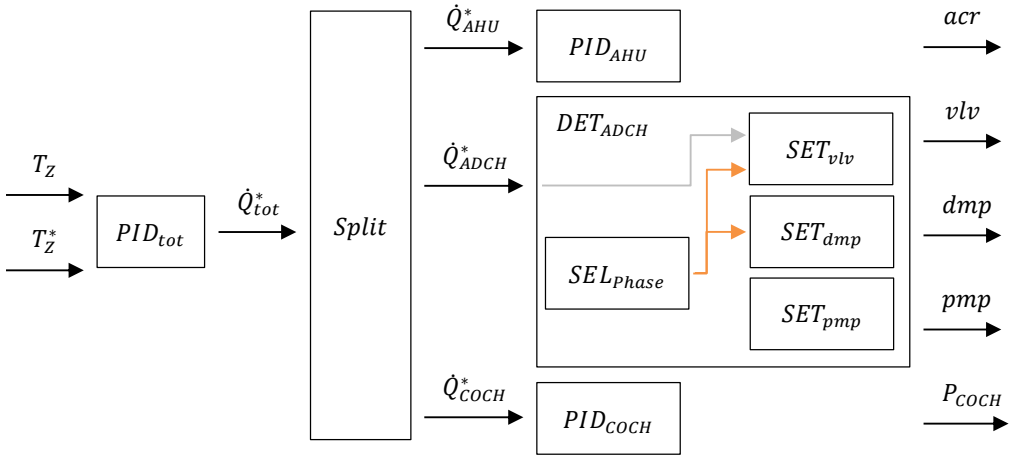

Figure 3: Schematic illustration of the control concept, set points with *

The second obd-approach (optimisation-based) switches the phase number based on predefined points in time. The phase also starts at phase 1 and changes from 1 to 2 at time t_{12}. For the subsequent switching times, the variables t_{23} and t_{34} were also introduced. The optimal times were determined for each set of configuration parameters such that the total energy consumption is minimal. To obtain the total energy consumption for a parameter set, the entire model was exported as an fmu-model and simulated in Python with fmpy. The optimal energy consumption under variation of the time variables was achieved by coupling the fmu-model with the solver scipy-optimize-minimize, using the Powell method.

2.5. Parameter variation

To verify the third central hypothesis of this work, the parameters that decisively influence the cooling performance of the façade-integrated adsorption cooling are varied and optimised in addition to the operating strategy. From the set of system parameters, 6 parameters were identified and reduced to 2 parameters. The parameters include the position of the adsorber or_{ads} and condenser or_{con}, the facade area ratios of adsorber f_{ads} and condenser f_{con}, the floor area ratio of the evaporator f_{eva} and the azimuthal building orientation γ_{build}.

The façade area ratios f_{ads}, f_{con} are limited by the defined areas of the windows and the total area. Each orientation has one window with the area ratio $f_{win} = 0.25$. The sum condition must hold for each orientation: $f_{ads} + f_{con} + f_{win} + f_{wal} = 1$. The façade area of the lightweight wall type f_{wal} is adjusted so that the condition is fulfilled. The façade area ratios are proportional to the mass of zeolite and the heat exchange area of all three components. In this work the area ratios are set equal, $f_{ads} = f_{con} = f_{eva} = f$. This scales the cooling capacities and exchange areas together. However, this reduction in complexity prevents the identification of dominant cooling capacity limitations.

To consider a maximum angular range of the adsorber orientation γ_{ads}, the adsorber is always placed in the position $or_{ads} = 1$. The positions $or_j = \{1,2,3,4\}$ correspond to a south, west, north or east orientation, respectively, as long as the building is oriented towards the south $\gamma_{build} = 180°$. By varying the building orientation γ_{build}, the adsorber orientation γ_{ads} changes to the same extent. The condenser is always placed in position 3 since the modelling of the condenser does not yet include any interaction with solar irradiance and the north orientation is dominated by shadow.

In summary, this paper considers the system efficiency analysis with respect to the façade area ratio f and the adsorber orientation γ_{ads}.

To obtain comparable energy consumptions, the initial temperatures of the room, adsorber, condenser and evaporator were set to a fixed value ($T_Z = T_E = 24.3°C, T_A = 47.2°C, T_C = 25.7°C$). The initial value of the loading was chosen to satisfy the periodicity condition ($|x_{ads}(t = 0) - x_{ads}(t = 24h)| < 10^{-4}$). This condition was achieved by iteratively setting the final value of the loading to the initial value until it was satisfied. This periodicity condition was applied to both operating strategies individually.

3. Results & Discussion

3.1. Comparison of the operating strategy

To visualize the influence of the different operating strategies, the time trends in Figure 4 are used first. These show the operating phases, the adsorber loading and the current cooling capacity for both operating strategies. In this context, all area ratios are set to the value $f = 0.5$ and the building is oriented in south-southeast direction $\gamma_{ads} = 160°$ like the D1244.

The phase curve depicted in Figure 4 shows that by using the obd-strategy, desorption starts later, intercooling and the cooling phase start earlier. Along with the delayed start of desorption, there is no premature increase in loading as with the rbd-operating strategy. This increase in the desorption phase leads to opposite mass flows from the condenser to the adsorber and, as a result of its temperature increase, to lower cooling capacity. Flap

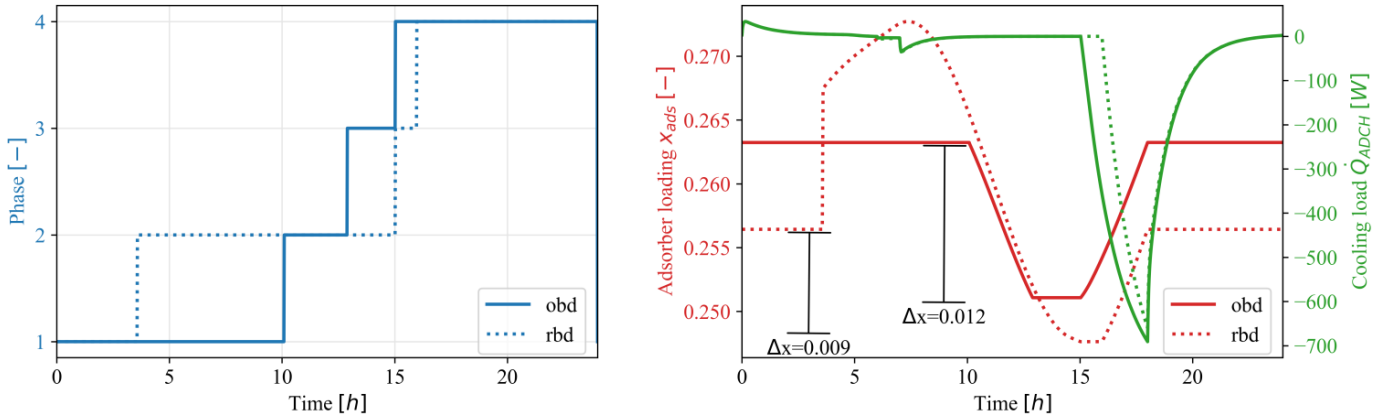

Figure 4: Time behaviour of the operating phases (left) and the adsorber loading x_{ads} and cooling capacity $\dot{Q}_{ADCH}$ (right) in comparison to both operating strategies

valves could be used to stop the backflow. The loading difference for the obd operating strategy is slightly larger, although the initial loading is larger. The cooling capacity drops earlier according to the earlier switching time t_{34} and reaches a higher cooling load as with the rbd-strategy. The slightly increased loading difference in combination with the avoidance of backflows and the earlier start of the cooling phase finally leads to a higher cooling energy and 5.6% lower total electricity consumption E_{tot}.

Next, the dependence of the total energy consumption E_{tot} on the building orientation and the operating strategy was investigated, cmp. Figure 5. As before, the area ratios were set to f=0.5.

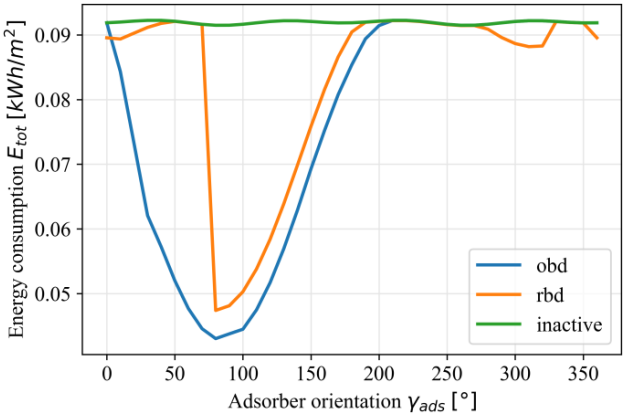

Figure 5: Total daily energy consumption E_{tot} versus adsorber orientation γ_{ads} with varying operating strategy.

The green curve results from an overall model with an inactive adsorption cooling system. In this case, the phase is kept constant at 1. This curve shows that the solar energy gains uniformly occur across all building orientations. This depends solely on the distribution of the windows across the building orientations. In comparison, the energy consumptions with active adsorption cooling system are consistently lower. The total energy consumption with rbd-operating strategy drops very sharply from a threshold orientation in the range of $\gamma_{ads} \in \{70°, 80°\}$. Prior to this threshold orientation, the switching condition from phase 4 to 1 holds at noon instead of in the morning on the following day due to a short and small increase in solar irradiation. As a result, the cooling phase, and the associated cooling power $\dot{Q}_{ADCH}$ are lower in this range, and the total power consumption is significantly higher. Compared to the rbd-operating strategy, the obd-operating strategy enables lower energy consumption in the predominant range. Most importantly, it enables efficient operation in the range below the threshold orientation. In the range of west orientation $\gamma_{ads} > 180°$, the rbd-operation strategy is slightly more suitable. Its curve shows a second smaller minimum. Due to an early switchover to phase 1 or 2 at noon, the loading is desorbed in the evening. As a result, the load unexpectedly increases in the morning and decreases in the evening, the loading lift is reversed. The obd-operating strategy is not able to perform a reverse loading lift due to the fixed switchovers and fixed initial phase. A slight adjustment by coupling the initial phase and phase development to the building

orientation could offer significant advantages for both operation strategy for western adsorber orientations.

3.2. Comparison of the system parameter

To eliminate the small fluctuation of the energy consumption when the adsorption cooling is inactive with the adsorber orientation, cmp. Figure 5 green line, the relative difference to the consumption with an active adsorption cooling system is considered. These relative energy consumption reductions are shown in Figure 6 for both operating strategies and for a variable facade area ratio f. The facade area ratio is varied up to a maximum value of $f_{max} = 0.75$.

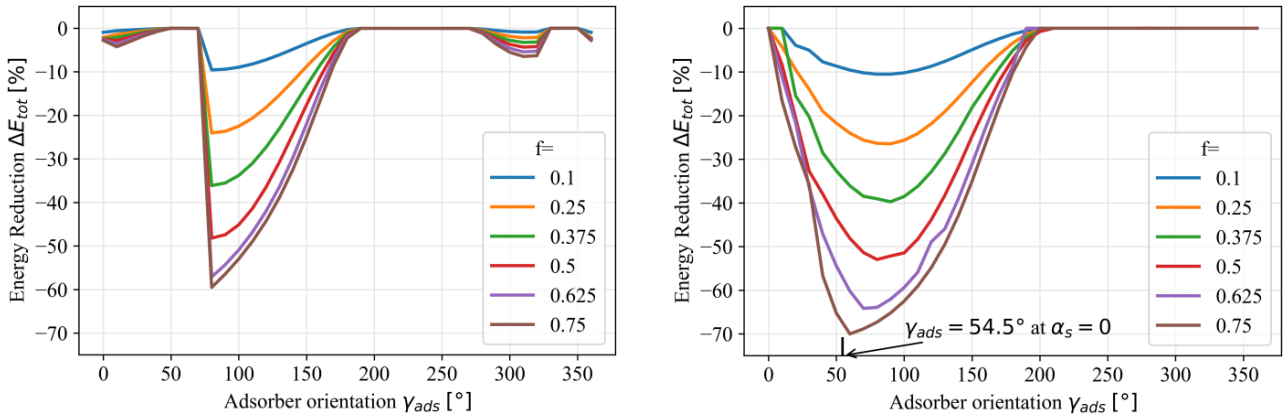

Figure 6: Energy savings by using facade-integrated adsorption cooling and by using the rbd-operating strategy (left) or obd-operating strategy compared to the azimuthal orientation of the adsorber γ_{ads} with variable facade area ratio f

The energy reduction curve is similar to that of the absolute total electricity consumption in Figure 5, since the reference value with inactive adsorption cooling systems is nearly constant. Accordingly, the energy savings applying the rbd-operating strategy reveals the same drop as in the previously discussed results. Now it is shown that this threshold orientation is the same for all area ratios. This is because the switching criterion depends only on the solar radiation. As Figure 7 (left) clarifies for obd-strategy, the reduction in consumption decreases proportionally with the facade area ratio up to a ratio of $f = 0.6$. With the increasing area ratios, the adsorbate quantity and the heat exchange areas increase, providing more cooling capacity. From an area ratio $f = 0.6$ the reduction decreases less and the optimum shifts to the solar azimuth at sunrise $\gamma_{ads} = 54.5°$. As Figure 8 reveals, the adsorption cooling system now takes over the complete cooling task. The compression cooling is reduced. A further saving is thus only possible if the desorption and thus the adsorption starts earlier. This angle change is also illustrated in Figure 7 (left). Figure 7 (right) shows the switching times for obd-strategy versus building orientation for all possible facade area ratios. In the range from the solar azimuth at sunrise to the south orientation $54.5° < \gamma_{ads} < 180°$ all curves cluster into three nearly distinct lines. These describe from bottom to top the

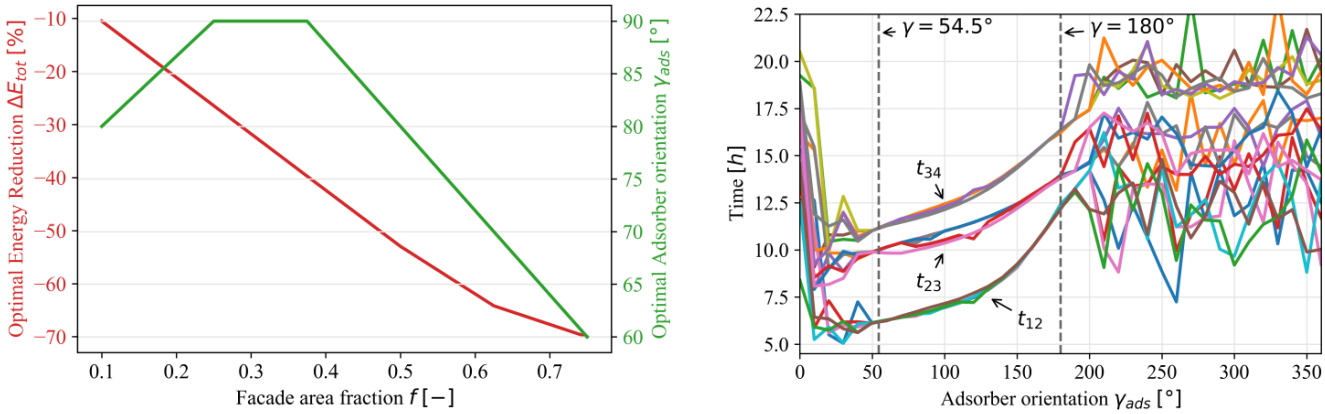

Figure 7: Left: Optimal energy reduction ΔE_{tot} and adsorber orientation γ_{ads} versus facade area ratio f, Right: Switching times between phases versus adsorber orientation γ_{ads} at all facade area ratios, both subfigures for obd-strategy

switching times t_{12}, t_{23}, t_{34} versus the adsorber orientation. In this range, the switching times are nearly independent of the facade area ratio. In the range $54.5° > \gamma_{ads} > 180°$ there is no unique clustering. In this range, the obd-operating strategy does not provide unique switching times. However, these uncertainties do not affect the curves of the energy reduction in Figure 6. It remains open whether this is the result of purely numerical or also physical reasons.

Figure 8 shows the time curves of the loading, the total cooling power $\dot{Q}_{tot}$, the cooling power by the compression cooling $\dot{Q}_{COCH}$ as well as that of the adsorption cooling $\dot{Q}_{ADCH}$, each for initial (init, $f = 0.5, \gamma_{ads} = 160°$) and the optimal parameter set (opti, $f = 0.75, \gamma_{ads} = 60°$).

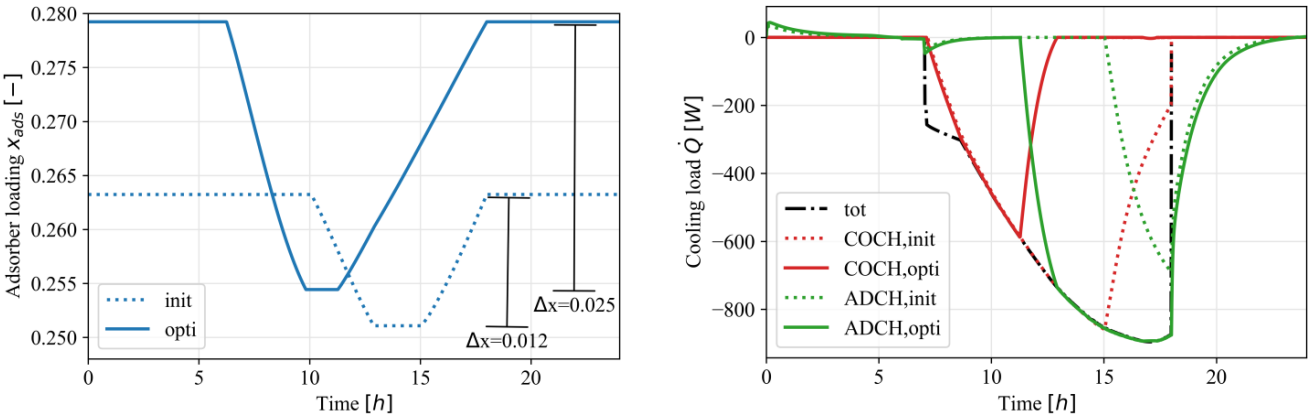

Figure 8: Time curves of the operating phases (left) and of the adsorber loading x_{ads} and cooling capacities $\dot{Q}$ (right) with obd-operating strategy in comparison between the initial and optimal parameter set.

The loading stroke with an optimum parameter set is more than twice as large as in the comparison case. The cooling demand at the beginning of the working time is covered by the ventilation if the outside temperature is lower than the upper room temperature limit at $24°C$. Thereafter, the adsorption and compression cooling system are added. In the optimum case, the cooling load is taken over by the adsorption cooling system at about 1 p.m., about 5 hours earlier. The course of the cooling capacity by the compression cooling system is shifted to the morning hours. Accordingly, a second, perhaps small adsorption cooling system in a western orientation would be suitable to cool the system completely emission-free.

4. Conclusion

In this paper, a new optimization-based operation strategy and an efficiency analysis on a novel façade-integrated adsorption cooling system were presented. The main contributions of this work are as follows:

By applying the obd-operation strategy, energetically more optimal switching times can be found compared to the rbd-operation strategy. By applying optimal system parameters and the obd-strategy, power consumption can be reduced by additional 10% compared to the rbd-strategy. This confirms the first hypothesis of this work. Applying the obd-strategy shows a distinct minimum of total electricity consumption with building orientation and area ratios. This confirms the second central hypothesis. In comparison, the rbd-operating strategy can only be applied up to a certain threshold orientation, which was attributed to a switching condition. In contrast, it allows for a small second minimum of energy reduction in the western orientation region. This reveals that the coupling of the switching criteria to the adsorber orientation is indispensable. The time behaviour of the solar energy gains is defined by the area ratios of the windows and the dimensions of the building. Accordingly, the location of the optimal parameter configuration (building orientation, component area ratio) is coupled to it. However, under the assumptions of this work, which among other things provides for a uniform distribution of the windows and certain facade dimensions, the optimal orientation of the adsorber is $\gamma_{ads} = 60°$, and the optimal facade area ratio is $f = 0.75$. In this case, the total electricity consumption can be reduced by 70% through the novel facade-integrated adsorption cooling.

Future work should further develop the obd-operation strategy so that the phase selection is coupled to the adsorber orientation and thus it can optimally operate the system in both orientations. Accordingly, it must be

investigated to what extent the additional compression cooling machine can be dispensed with by using a second adsorber-condenser system in the opposite orientation. In this case, the coordination between the components becomes much more challenging as the interconnection possibilities between the components increase. This can make the application of model-predictive control concepts necessary. Here, it must be investigated to what extent the loading is suitable as a unique and continuous manipulated variable for each adsorber system. In this work all area ratios were kept equal. To overcome this condition should be part of future work. Thereby, threshold values for heat transfer barriers could be investigated and considered in the design.

5. Acknowledgements

This work was carried out within the Collaborative Research Centre CRC1244 ‘Adaptive skins and structures for the built environment of tomorrow’ subproject C06, which are funded by the German Research Foundation under the Project-ID 279064222.

6. References

Almasri, R.A., Abu-Hamdeh, N.H., Esmaeil, K.K., Suyambazhahan, S., 2022. Thermal solar sorption cooling systems - A review of principle, technology, and applications. Alexandria Engineering Journal 61, 367–402. https://doi.org/10.1016/j.aej.2021.06.005

Blandini, L., Haase, W., Weidner, S., Böhm, M., Burghardt, T., Roth, D., Sawodny, O., Sobek, W., 2022. D1244: Design and Construction of the First Adaptive High-Rise Experimental Building. Frontiers in Built Environment 8.

Boeckmann, O., Schaefer, M., 2021. Modellierung und Simulation eines fassadenintegrierten Adsorptionssystems zur solaren Gebäudekühlung. DECHEMA Thermodynamik Kolloquium, Chemnitz

Curcija, C., Vidanovic, S., Hart, R., Jonsson, J., Powles, R., 2018. WINDOW Technical Documentation 220.

DIN V 18599-10:2018-09, Energetische Bewertung von Gebäuden_- Berechnung des Nutz-, End- und Primärenergiebedarfs für Heizung, Kühlung, Lüftung, Trinkwarmwasser und Beleuchtung-Teil 10: Nutzungsrandbedingungen, Klimadaten, n.d.. Beuth Verlag GmbH. https://doi.org/10.31030/2874436

Heidingsfeld, J.L., Boeckmann, O., Schaefer, M., Böhm, M., Sawodny, O., 2022. Low Order Hybrid Model for Control Design. CCTA Conference, Trieste

Jorissen, F., Reynders, G., Baetens, R., Picard, D., Saelens, D., Helsen, L., 2018. Implementation and verification of the IDEAS building energy simulation library. Journal of Building Performance Simulation 11, 669–688. https://doi.org/10.1080/19401493.2018.1428361

Müller, D., Lauster, M., Constantin, A., Fuchs, M., Remmen, P., n.d. AIXLIB – AN OPEN-SOURCE MODELICA LIBRARY WITHIN THE IEA-EBC ANNEX 60 FRAMEWORK 8.

Nytsch-Geusen, C., Huber, J., Ljubijankic, M., Rädler, J., 2013. Modelica BuildingSystems − eine Modellbibliothek zur Simulation komplexer energietechnischer Gebäudesysteme. Bauphysik 35, 21–29. https://doi.org/10.1002/bapi.201310045

Prieto, A., Knaack, U., Auer, T., Klein, T., 2017. Solar coolfacades: Framework for the integration of solar cooling technologies in the building envelope. Energy 137, 353–368. https://doi.org/10.1016/j.energy.2017.04.141

Settino, J., Sant, T., Micallef, C., Farrugia, M., Spiteri Staines, C., Licari, J., Micallef, A., 2018. Overview of solar technologies for electricity, heating and cooling production. Renewable and Sustainable Energy Reviews 90, 892–909. https://doi.org/10.1016/j.rser.2018.03.112

UN 2021 Status Report, United Nations Environment Programme (2021) 2021 Global Status Report for Buildings and Construction: Towards a Zero-emissions, Efficient and Resilient Buildings and Construction Sector – Full report. Available at: https://www.unep.org/resources/report/2021-global-status-report-buildings-and-construction (Accessed: 8 September 2022)

Wetter, M., Zuo, W., Nouidui, T.S., Pang, X., 2014. Modelica Buildings library. Journal of Building Performance Simulation 7, 253–270. https://doi.org/10.1080/19401493.2013.765506